A New Lipid Anchor for Sparsely Tethered Bilayer Lipid Membranes†

Frank Heinrich,[‡,||] Tiffany Ng,[⊥] David J. Vanderah,[§] Prabhanshu Shekhar,[||] Mihaela Mihailescu,[‡,#] Hirsh Nanda,[‡] and Mathias Lösche*[,‡,||]

Center for Neutron Research, National Institute of Standards and Technology, Gaithersburg, Maryland 20899-6102, Chemical Sciences and Technology Laboratory, National Institute of Standards and Technology, Gaithersburg, Maryland 20899-8313, Physics Department, Carnegie Mellon University, Pittsburgh, Pennsylvania 15213-3890, Department of Biomedical Engineering, Johns Hopkins University, Baltimore, Maryland 21218, and Department of Physiology and Biophysics, School of Medicine, University of California at Irvine, Irvine, California 92697

Received October 8, 2008. Revised Manuscript Received December 11, 2008

Mixed self-assembled monolayers (SAMs) of β-mercaptoethanol and the new synthetic lipid 1,2-dipalmityl-3-[ω-mercaptonona(ethylene oxide)] glycerol (FC16) were investigated for their ability to form sparsely tethered bilayer lipid membranes (stBLMs) completed with various phospholipids. We investigated the structural and functional properties of FC16-based stBLMs and compared these to stBLMs prepared using a previously characterized synthetic lipid, 1,2-dimyristyl-3-[ω-mercaptohexa(ethylene oxide)] glycerol (WC14). FC16-based stBLMs show increased resistivity to ion transfer and an increase in the submembrane space of ∼0.5 nm. Importantly, FC16-based stBLMs formed well-defined, complete bilayers with charged phospholipids such as 1-palmitoyl-2-oleoyl-*sn*-glycero-3-phosphoglycerol (POPG). In these, POPG incorporates into the outer monolayer leaflet in the same ratio as in the immersion solution but is excluded from the inner leaflet. In all cases that we have investigated thus far, the area densities of the lipids within the bilayers were on average close to those in free bilayer membranes. For charged phospholipids, FC16 appears to provide a distinct advantage over WC14 for the formation of well-defined stBLMs.

I. Introduction

Protein crystallography has revolutionized our understanding of molecular biology and is the technique of choice for determining protein structures with full atomic detail. Nevertheless, many relevant functional biological entities are in the form of disordered structures that require other techniques, such as nuclear magnetic resonance (NMR) or neutron reflectometry (NR), for their investigation. A particularly important example of a biologically active, disordered structure is the lipid bilayer membrane, a double-layer leaflet of fluid lipids that provides the context for the function of membrane proteins that reside in them.[1,2] Although the lipid bilayer is in-plane disordered and merely ∼5 nm thick, it is highly insulating against ion transport across the membrane, which is key to many vital biological functions from charge separation in photosynthesis to signal conduction along neuronal axons.

To investigate the physical properties of lipid bilayers on the molecular scale, model membranes have been employed for decades. Starting with work by McConnell's group,[3,4] bilayer models supported by solid substrates have been investigated as membrane mimics. We and others[5−10] have more recently developed tethered bilayer membrane (tBLM) systems on solid supports that are separated from the inorganic surface by an ultrathin hydration layer. tBLMs take advantage of planar geometry brought about by the solid support to study molecular interactions of proteins with lipid bilayers in a system that is resilient and fluid in-plane. Typically, a synthetic lipid anchor, which tethers one or more hydrophobic chains via a hydrophilic spacer such as an oligo(ethylene oxide), is chemisorbed to the substrate surface.

Cornell and co-workers developed a tBLM system with incorporated synthetic gramicidin derivatives that modulated ion flux across the membrane by biospecific binding of analytes, thus converting chemical into electric signals.[5] In their seminal work, they developed a technique for bilayer completion that bypassed the frequently used vesicle fusion approach with a process termed "rapid solvent exchange". In this process, a self-assembled monolayer (SAM) of the tether lipid is incubated with an organic solution of lipids, followed by rapid replacement of the organic phase by aqueous buffer. This procedure precipitates a bimolecular layer onto the SAM that mimics well most aspects of a lipid membrane. As has been shown with NR,[10−13] rapid solvent exchange intercalates lipids between the tethers in the

† Part of the Neutron Reflectivity special issue.

* Corresponding author. E-mail: quench@cmu.edu. Tel: 412-268-2735. Fax: 412-268-8252.

‡ Center for Neutron Research, National Institute of Standards and Technology.

§ Chemical Sciences and Technology Laboratory, National Institute of Standards and Technology.

|| Carnegie Mellon University.

⊥ Johns Hopkins University.

University of California at Irvine.

(1) Rietveld, A.; Simons, K. *Biochim. Biophys. Acta* **1998**, *1376*, 467–479.

(2) Singer, S. J.; Nicolson, G. L. *Science* **1972**, *173*, 720–731.

(3) Brian, A. A.; McConnell, H. M. *Proc. Natl. Acad. Sci. U.S.A.* **1984**, *81*, 6159–6163.

(4) Tamm, L. K.; McConnell, H. M. *Biophys. J.* **1985**, *47*, 105–113.

(5) Cornell, B. A.; Braach-Maksvytis, V. L. B.; King, L. B.; Osman, P. D. J.; Raguse, B.; Wieczorek, L.; Pace, R. J. *Nature* **1997**, *387*, 580–583.

(6) Sackmann, E. *Science* **1996**, *271*, 43–48.

(7) Stora, T.; Lakey, J. H.; Vogel, H. *Angew. Chem., Int. Ed.* **1999**, *38*, 389–392.

(8) Knoll, W.; Frank, C. W.; Heibel, C.; Naumann, R.; Offenhäuser, A.; Rühe, J.; Schmidt, E. K.; Shen, W. W.; Sinner, A. *Rev. Mol. Biotechnol.* **2000**, *74*, 137–158.

(9) Tanaka, M.; Sackmann, E. *Nature* **2005**, *437*, 656–663.

(10) McGillivray, D. J.; Valincius, G.; Vanderah, D. J.; Febo-Ayala, W.; Woodward, J. T.; Heinrich, F.; Kasianowicz, J. J.; Lösche, M. *Biointerphases* **2007**, *2*, 21–33.

(11) Valincius, G.; McGillivray, D. J.; Febo-Ayala, W.; Vanderah, D. J.; Kasianowicz, J. J.; Lösche, M. *J. Phys. Chem. B* **2006**, *110*, 10213–10216.

(12) Valincius, G.; Heinrich, F.; Budvytyte, R.; Vanderah, D. J.; McGillivray, D. J.; Sokolov, Y.; Hall, J. E.; Lösche, M. *Biophys. J.* **2008**, *95*, 4845–4861.

(13) McGillivray, D. J.; Valincius, G.; Heinrich, F.; Robertson, J. W. F.; Vanderah, D. J.; Febo-Ayala, W.; Ignatjev, I.; Lösche, M.; Kasianowicz, J. J. *Biophys. J.*, 2008, in press.

10.1021/la8033275 CCC: $40.75
Published on Web 02/12/2009

Scheme 1. Synthesis of FC16[a]

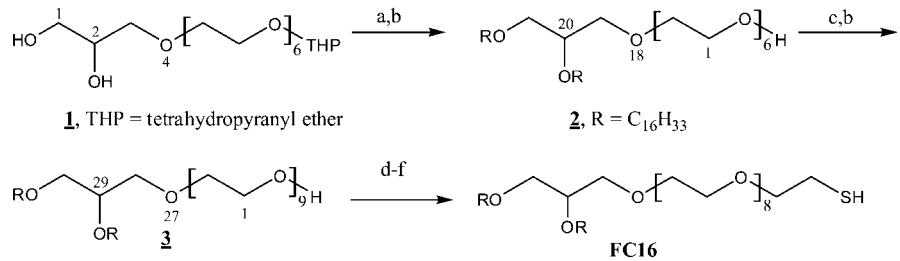

[a] (a) 3 equiv of NaH/THF, followed by 3 equiv of $C_{16}H_{33}Br$, 42 °C, 3 days, 65%. (b) CH_3CO_2H/THF/H_2O (4/2/1), 50 °C, 7 h, 68%. (c) NaH/THF, followed by $Cl(CH_2CH_2O)_3THP$, 45 °C, 5 days, 55%. (d) $(C_6H_5)_3P$ then *N*-bromosuccinimide, CH_2Cl_2, 12 h, RT, 89%. (e) $CH_3COS^-Na^+/CH_3OH$, 7 h, 80%. (f) 1 N HCl/CH_3OH, reflux, 8 h, 90%.

monolayer proximal to the substrate and complements this proximal layer with a distal monolayer of lipid, thus rendering the surface hydrophilic. Phospholipids reside in this bilayer in a lateral density similar to that of lipids in free-standing bilayers, such as vesicles. Importantly, such tBLMs usually have higher electrical resistance[10,14] and a lower defect density[10] than bilayers prepared by vesicle fusion. NR also shows unambiguously that a thin (∼1 nm), stable hydration layer separates the proximal lipid monolayer from the solid substrate. Such a layer is deemed important for rendering the in-plane bilayer fluid and providing space for the insertion of transmembrane proteins into the synthetic bilayer model.

In earlier work with a specific anchor lipid, 1,2-dimyristyl-3-[ω-mercaptohexa(ethylene oxide)] glycerol (WC14), we optimized such bilayer architecture formed on molecularly smooth Au films by recognizing that it is essential to dilute the grafting points laterally with a short hydrophilic "backfiller",[14] such as β-mercaptoethanol (βME). We refer to the resulting membrane mimics as sparsely tethered bilayer lipid membranes (stBLMs).

The resilience of the tBLM system may be demonstrated in various ways. For tBLMs completed with diphytanoylphosphatidylcholine, which forms particularly dense, yet fluid bilayers, Köper and co-workers showed that such membranes can withstand electrical dc fields of up to several 10^8 V/cm.[15] Remarkably, the electrical parameters of such bilayers were shown to be stable for months.[15]

For characterization with NR, we routinely take advantage of this resilience by performing a multitude of measurement scans on one physical sample under multiple solvent contrasts and/or comparing the as-prepared tBLM structure with its structure under the influence of a ligand, such as a protein. For example, we have recently incorporated a bacterial toxin, α-hemolysin (αHL), at extremely high density into the tBLM and have characterized the structure of the resulting protein-reconstituted membrane.[13] Not only does the bilayer withstand various solvent exchanges between consecutive measurements but it is also stable if perforated by a lysogenic protein such as αHL at a density of $>10^3/\mu m^2$. Because all sample manipulations are performed in situ on the sample cell of the neutron instrument, consecutive NR measurements are made on identical footprints of the neutron beam on the sample. NR emerges, therefore, as a prime tool for the determination of intrinsically disordered structures, such as an in-plane fluid bilayer, at a (1D) resolution that approaches 1 Å.[13] Reflectivity measurements of polarized neutrons reflected from substrates that carry magnetic nanolayers buried underneath the gold film have recently been shown to achieve even higher resolution on extremely thin organic films.[16]

tBLM systems offer application potential in a broad range of biomedical investigations where the interaction of proteins with membranes is of immediate interest, such as studies in toxicology,[13,17] Alzheimer's disease,[12] cell signaling involving lipids,[18] and laminopathies.[19] In this work, we describe a new lipid anchor, FC16 {1,2-dipalmityl-3-[ω-mercaptonona(ethylene oxide)] glycerol}, that we developed on the basis of WC14, in its molecular architecture and describe it ability to form stBLMs.

II. Experimental Section[20]

Synthesis of FC16. The preparation of FC16 (IUPAC: 29-hexadecyloxy-3,6,9,12,15,18,21,24,27,31-decaoxaheptatetracontan-1-thiol) was initiated with the tetrahydropyranyl ether of 4,7,10,13,16,19-hexaoxaheneicosan-2,21-diol (**1**) (Scheme 1), which is available as an intermediate in the previously described synthesis of WC14,[10] and proceeded through the alkylation of the vicinal 1,2-dihydroxy groups, deprotection, ethylene oxide chain extension via Williamson ether synthesis using the tetrahydropyranyl ether of the commercially available 2-[2-(2-chloroethoxy) ethoxy]ethanol, deprotection, and conversion of the newly generated, terminal hydroxyl group to the thiol as described previously.[21]

Synthesis. Tetrahydrofuran (THF) (Mallinckrodt AR) and 2-[2-(2-chloroethoxy)ethoxy]ethanol were purchased from North Strong Scientific (Phillipsburg, NJ) and TCI (Portland, OR), respectively. THF was distilled from CaH_2 immediately before use. All other chemicals were purchased from Aldrich (Milwaukee, WI) and used as received. All compounds were purified by chromatography [silica gel, J. T. Baker (Phillipsburg, NJ), 40 μm, column = 33 cm × 3 cm]. ^{1}H NMR spectra were obtained on a JEOL 270 MHz spectrometer in $CDCl_3$ containing 0.03% tetramethylsilane (TMS). Chemical shifts (δ) are in parts per million (ppm) relative to TMS, and coupling constants (J) are in Hertz (Hz). All reactions were carried out under nitrogen.

*Tetrahydropyranyl Ether of 20-Hexadecyloxy-3,6,9,12,15,18,22-heptaoxaoctatricontan-1-ol (**2**-THP).* To 0.192 g (8.0 mmol) of NaH in 3 mL of THF was added 1.11 g (2.51 mol) of **1** in 5 mL of THF at room temperature. After the completion of the addition, the temperature was increased to 42 °C, and 2.67 g (8.7 mmol) of 1-bromohexadecane in 8 mL of THF was added dropwise. After 3 days at 42 °C, the mixture was filtered, adsorbed onto 7 g of silica gel, and chromatographed (100% ethyl acetate) to give 0.615 g of

(14) Raguse, B.; Braach-Maksvytis, V. L. B.; Cornell, B. A.; King, L. B.; Osman, P. D. J.; Pace, R. J.; Wieczorek, L. *Langmuir* **1998**, *14*, 648–659.
(15) Vockenroth, I. K.; Ohm, C.; Robertson, J. W. F.; McGillivray, D. J.; Lösche, M.; Köper, I. *Biointerphases* **2008**, *3*, FA68−FA73.
(16) Holt, S. A.; Le Brun, A. P.; Majkrzak, C. F.; McGillivray, D. J.; Heinrich, F.; Lösche, M.; Lakey, J. H. *Soft Matter* 2008, submitted.
(17) Kent, M. S.; Yim, H.; Murton, J. K.; Satija, S.; Majewski, J.; Kuzmenko, I. *Biophys. J.* **2008**, *94*, 2115–2127.
(18) Wymann, M. P.; Schneiter, R. *Nat. Rev. Mol. Cell Biol.* **2008**, *9*, 162–176.
(19) Liu, B.; Zhou, Z. *Histol. Histopathol.* **2008**, *23*, 747–63.
(20) Certain commercial materials, equipment, and instruments are identified in this manuscript in order to specify the experimental procedure as completely as possible. In no case does such an identification imply a recommendation or endorsement by the National Institute of Standards and Technology, nor does it imply that the materials, equipment, or instruments identified are necessarily the best available for the purpose.
(21) Vanderah, D. J.; Valincius, G.; Meuse, C. W. *Langmuir* **2002**, *18*, 4674–4680.

2-THP. ^{1}H NMR: δ 4.63 (1 H, br. t, J = 3.0, tetrahydropyranyl OC**H**O methine), 0.88 (6 H, br. t, J = 6, 2 C**H**$_3$C$_{15}$H$_{30}$O). Chromatography also afforded 0.186 g of a more polar monoalkylated product, most likely 3,6,9,12,15,18,22-heptaoxaoctatricontane-1,20-diol. ^{1}H NMR: δ 4.63 (1 H, br. t, J = 3.0, tetrahydropyranyl OC**H**O methine), 0.88 (3 H, br. t, J = 6, C**H**$_3$C$_{15}$H$_{30}$O).

20-Hexadecyloxy-3,6,9,12,15,18,22-heptaoxaoctatricontan-1-ol (**2**). A solution of 1.05 g (1.2 mmol) of **2**-THP in 28 mL of glacial acetic acid/THF/water (4/2/1) was maintained at 50 °C for 7 h. The removal of solvents and chromatography (5% methanol/ethyl acetate) afforded 0.644 g (68%) of **2**. ^{1}H NMR: δ 3.9 to 3.4 (33 H, m, −C**H**$_2$C**H**$_2$O− and −C**H**O− protons, 2.6 (0.8 H, br. t, RO**H**), 1.55 (4 H, br. pentet, $J \approx 6$, 2 C$_{14}$H$_{27}$C**H**$_2$CH$_2$O−), 1.25 (52 H, br. s, 2 C$_{14}$**H**$_{27}$CH$_2$CH$_2$O−), 0.88 (6 H, br. t, $J \approx 6$, 2 C**H**$_3$C$_{15}$H$_{30}$O).

*Tetrahydropyranyl Ether of 29-Hexadecyloxy-3,6,9,12,15,18,21,24,27,31-decaoxaheptatetracontan-1-ol (**3**-THP).* To 0.11 g (4.6 mmol) of NaH in 3 mL of THF was added 0.644 g (0.8 mmol) of **2** at 0 °C. After the completion of the addition, the temperature was increased to 43 °C. To this solution was added 1.09 g (4.3 mmol) of Cl(CH$_2$CH$_2$O)$_3$THP in 6 mL of THF, and the resulting solution was maintained at 43 °C for 5 days. Water (50 mL) was added, cautiously at first, and THF was removed under reduced pressure. The aqueous layer was continuously extracted with ethyl acetate overnight. Chromatography of the ethyl acetate residue (5% methanol/ethyl acetate) yielded 0.585 g (78%) of **3**-THP. ^{1}H NMR: δ 4.63 (1 H, br. t, $J \approx 3.0$, tetrahydropyranyl OC**H**O methine), 3.9 to 3.4 (47 H, −C**H**$_2$C**H**$_2$O− and −C**H**O− protons), 0.88 (6 H, br. t, $J \approx$ 6, 2 C**H**$_3$C$_{15}$H$_{30}$O).

29-Hexadecyloxy-3,6,9,12,15,18,21,24,27,31-decaoxaheptatetracontan-1-ol (**3**). A solution of 0.585 g (0.57 mmol) of **3**-THP in 28 mL of glacial acetic acid/THF/water (4/2/1) was maintained at 50 °C for 8 h. The removal of solvents and chromatography (10% methanol/ethyl acetate) afforded 0.466 g (78%) of **3**. ^{1}H NMR: δ 3.9 to 3.4 (45 H, m, −C**H**$_2$C**H**$_2$O− and −C**H**O− protons, 2.6 (0.8 H, br. t, RO**H**), 1.55 (4 H, br. pentet, $J \approx 6$, 2 C$_{14}$H$_{27}$C**H**$_2$CH$_2$O−), 1.25 (52 H, br. s, 2 C$_{14}$**H**$_{27}$CH$_2$CH$_2$O−), 0.88 (6 H, br. t, $J \approx 6$, 2 C**H**$_3$C$_{15}$H$_{30}$O).

30-Bromo-1,2-dihexadecyloxy-4,7,10,13,16,19,22,25,28-tricontane (**4**). To a solution of 0.466 g (0.50 mmol) of **3** and 0.1572 g (0.60 mmol) of triphenylphosphine in 7 mL of dry CH_2Cl_2 was added 0.1067 g (0.6 mmol) of *N*-bromosuccinimide in small portions that were then stirred overnight at room temperature. Chromatography (5% methanol/ethyl acetate) gave 0.377 g (76%) of **4**. ^{1}H NMR: δ 3.81 (2 H, t, J = 6.5, BrC**H**$_2$CH$_2$), 0.88 (6 H, br. t, J $\approx$ 6, 2 C**H**$_3$C$_{15}$H$_{30}$O).

29-Hexadecyloxy-3,6,9,12,15,18,21,24,27,31-decaoxaheptatetracontan-1-thioacetyl (**5**). To 3 mL of CH_3OH was added 0.0014 g (0.62 mmol) of Na^0. After H_2 evolution ceased, 1.06 g (1.4 mmol) of CH_3COSH was added, followed by 0.377 g (0.377 mmol) of **4** in 5 mL of CH_3OH, and then the solution was refluxed for 7 h. Chromatography (5% methanol/ethyl acetate) yielded 0.351 g (94%) of **5** FC16-thiol acetate. ^{1}H NMR: δ 3.09 (2 H, t, J = 6.4, CH$_3$COSC**H**$_2$CH$_2$), 2.34 (3 H, s, C**H**$_3$COS), 0.88 (6 H, br. t, $J \approx 6$, 2 C**H**$_3$C$_{15}$H$_{30}$O).

29-Hexadecyloxy-3,6,9,12,15,18,21,24,27,31-decaoxaheptatetracontan-1-thiol (FC16). A solution of 0.351 g (0.35 mmol) of **5** was refluxed for 8 h in 30 mL of 0.1 N HCl/CH_3OH. Chromatography (3% methanol/ethyl acetate) afforded 0.308 g (92%) of pure FC16 (mp 33−35 °C). ^{1}H NMR: δ 3.7 to 3.4 (43 H, m, −C**H**$_2$C**H**$_2$O− and −C**H**O− protons), 2.70 (2 H, dt, $J \approx$ 6.5 and 6.2, HSC**H**$_2$CH$_2$O), 1.62 to 1.50 (5H, **H**S, 2 C$_{14}$H$_{27}$C**H**$_2$CH$_2$O−), 1.25 (52 H, br. s, 2 C$_{14}$**H**$_{27}$CH$_2$CH$_2$O−), 0.88 (6 H, br. t, $J \approx 6$, 2 C**H**$_3$C$_{15}$H$_{30}$O). High-resolution MS (ESI): m/z = 953.7621 (MH$^+$); calcd for C$_{53}$H$_{109}$O$_{11}$S: 953.7694.

Sample Preparation. Three-inch-diameter silicon wafers (100) from Silicon Quest Intl. Inc. (Santa Clara, CA) were coated with Cr (∼20 Å) and Au films (∼150 Å for neutron reflection and ∼500 Å for all other measurements) by high-energy magnetron sputtering (ATC Orion, AJA Intl., Inc., North Scituate, MA). Similar to earlier work with the related compound WC14, we prepared self-assembled monolayers (SAMs) by immersing freshly prepared Au film surfaces in 0.2 mmol/L ethanolic solutions of either FC16 or mixtures of FC16 and β-mercaptoethanol (βME; Sigma-Aldrich, St. Louis, MO) at different mol % ratios as specified, for example, as FC16/βME = 30:70. βME was distilled before use. After incubation, SAMs were rinsed with absolute ethanol and dried with nitrogen. Tethered lipid bilayer membranes (tBLMs) were formed by rapid solvent exchange as described.[10] Phospholipids used for the completion were 1,2-phytanoyl-*sn*-glycero-3-phosphocholine (DPhyPC), 1-palmitoyl-2-oleoyl-*sn*-glycero-3-phosphocholine (POPC), 1-palmitoyl-2-oleoyl-*sn*-glycero-3-phosphoglycerol (POPG or *h*-POPG), and 1-perdeuteropalmitoyl-2-oleoyl-*sn*-glycero-3-phosphoglycerol (d_{31}-POPG), all from Avanti Polar Lipids (Alabaster, AL) and used as supplied. Bilayers formed on mixed FC16/βME SAMs are henceforward referred to as sparsely tethered bilayer membranes (stBLMs) because βME dilutes the tether packing density at the Au surface, indicated, for example, by a more facile reconstitution of proteins into finished bilayers, as shown in previous work.[13]

Characterization Methods. Spectroscopic ellipsometry, Fourier transform infrared reflection−absorption spectroscopy (FT-IRRAS), contact angle measurements, and electrochemical impedance spectroscopy (EIS) were all performed at room temperature as previously described.[13,21] Multiple-wavelength ellipsometric measurements were performed on a J. A. Woollam Co., Inc. (Lincoln, NE) M-44 spectroscopic ellipsometer aligned at a nominal angle of incidence of ∼70° from the surface normal.[22]

p-polarized FT-IRRAS data were obtained using a Nicolet Magna-IR model 570 series II spectrometer (Thermo Nicolet, Madison, WI) with a model FT-85 (85° grazing angle with integrated polarizer) Spectra-Tech external reflection accessory (Thermo Spectra-Tech, Shelton, CT). The spectrometer utilized a KBr beamsplitter and a mercury cadmium telluride (MCT/A) detector. Spectra were acquired at 4 cm^{-1} resolution between 4000 and 700 cm^{-1} as a summation of 1000 scans using Happ-Genzel apodization without zero filling. Background spectra (R_o) were taken using [CD$_3$(CD$_2$)$_{17}$S]$_2$ SAMs on Au. The sample spectra (R) were acquired under identical equipment conditions and normalized by the background spectra to obtain spectra of $-\log(R/R_o)$ versus wavenumber.

Sessile contact angles (θ) were determined with a Ramé-Hart model 110-00-115 goniometer at ambient relative humidity using water as the probing liquid. At least four measurements were taken for each SAM by lowering a 2 to 3 μL drop onto the surface from a blunt-ended needle attached to a 2 mL syringe. The contact angle was recorded immediately after the drop detached from the needle tip.

EIS data were taken using a Solartron (Farnborough, U.K.) system (model 1287A potentiostat and model 1260 frequency response analyzer) and were fit to equivalent circuit models (ECMs) using ZView (Scribner Associates, Southern Pines, NC). Au-coated silicon wafers (20 × 40 mm^2) served as the working electrode in a setup that allowed simultaneous EIS measurements in six distinct electrochemical cells (volume, $V \approx 250-300$ μL) on each wafer, with their surface areas ($A_{el} \approx 0.33$ cm^2) on the Au film confined by Viton O-rings. Copper contrast was used to measure the geometric electrode surface area.[23] EIS data were normalized to A_{el} and the roughness factor β, estimated from the Au surface oxidation/oxide stripping charge.[24] A saturated silver−silver chloride (Ag|AgCl|NaCl(aq, sat)) microelectrode (Microelectrodes, Bedford, NH, model M-401F) was used as the reference. The auxiliary electrode was a 0.25-mm-diameter Pt wire (99.99% purity, Aldrich) coiled around the barrel of the reference electrode. The distance between the tip of the reference electrode and the working Au electrode surface was set to 2 to 3 mm. Measurements were carried out with 10 mV ac at 0 V bias versus the reference electrode in aerated solutions.

Neutron Reflection Data Acquisition and Analysis. Neutron reflectometry (NR) has been extensively used to characterize molecularly organized surfactant and lipid layers on the subnanometer

(22) Vanderah, D. J.; Arsenault, J.; La, H.; Gates, R. S.; Silin, V.; Meuse, C. W.; Valincius, G. *Langmuir* **2003**, *19*, 3752–3756.
(23) Vanderah, D. J.; Gates, R. S.; Silin, V.; Zeiger, D. N.; Woodward, J. T.; Meuse, C. W.; Valincius, G.; Nickel, B. *Langmuir* **2003**, *19*, 2612–2620.
(24) Trasatti, S.; Petrii, O. A. *Pure Appl. Chem.* **1991**, *63*, 711–734.

level.[25,26] NR measurements were performed on the Advanced Neutron Diffractometer/Reflectometer (AND/R)[27] at the NIST Center for Neutron Research (NCNR). The resilience of the stBLMs permitted the NR characterization of the membrane at various solvent contrasts with the same physical sample. For contrast variation, solvent exchange was performed in situ on the instrument so that the neutron spectra were taken on exactly the same footprints on the wafers. This ensured that the inorganic substrates, in particular, the SiO_x/Cr/Au surface layers that dominate the interference patterns in the data, contributed identically to subsequent measurements.

NR data analysis was performed using the optimization tool ga_refl,[28] developed at the NCNR. ga_refl supports the constrained fitting of multiple data sets in terms of slab models. Reflectivity is computed using an optical matrix.[29] ga_refl implements a genetic algorithm to perform a rapid search across parameter space with robustness against trapping in local minima. This genetic algorithm is alternated with a simplex amoeba algorithm.[30] The thus-obtained, preselected population of model parameters is further optimized using a Levenberg−Marquardt nonlinear least-squares fit. ga_refl supports the simultaneous fit of a set of reflectivity curves with shared parameters between the individual reflectivity curves. In general, all reflectivity curves measured on one and the same wafer in the course of a complex experiment are fitted simultaneously, sharing fit parameters, for example, for the substrate.

Data sets of isomorphic samples with distinct isotopic contrast were simultaneously fitted by refining the corresponding neutron scattering length density (nSLD) profiles $\rho_n(z)$ consistently with each other in terms of the underlying molecular structures.[26,31] The model contains the following sequence of layers along the direction, $\hat{z}$, of the surface normal: (semi-infinite) Si wafer, SiO_x, Cr, Au, the hydrated nona(ethylene oxide) spacer, the inner leaflet and the outer leaflet of the bilayer, the outer headgroup layer, and bulk solvent. The model allows all organic layers to comprise solvent, which contributes to the average scattering power of each layer according to the nSLD of the bulk solvent multiplied by its volume fraction in the layer (which may be zero in the hydrophobic core of a defect-free stBLM). Both lipid leaflets in the stBLM model were constrained to the same hydrophobic thickness because they are highly correlated. These two layers can, however, contain different amounts of water that may form solvent-filled defect pockets. The inner headgroup layer of the lipid membrane was indistinguishable from the nona(ethylene oxide) [NEO] tether at any solvent contrast and was therefore not separately modeled.

Parameter Confidence Analysis. A Monte Carlo (MC) resampling technique[30] was applied to determine fit parameter confidence intervals and parameter correlations. In this approach, a large number N (typically, $N = 1000$) of statistically independent sets of synthetic reflectivity data were created on the basis of the actual experimental data and their individual error bars (i.e., each synthetic reflectivity curve differed in each data point from the experimental reflectivity by a random normal deviate in which the width of the applied normal distributions is given by the uncertainty σ of the measured data point based on counting statistics). Each of the synthetic reflectivity data sets is simultaneously fitted using the algorithms described above, thus producing one set of fit parameters and a corresponding nSLD profile that deviate slightly from the "true" results but could have occurred given the experimental error bars associated with the actual measurement. A statistical analysis of all sets of fit parameters was applied to determine 95.4% confidence intervals by calculating the 2.3% and 97.7% percentiles of the parameter distributions. To assess parameter correlations, the covariance for any given pair of fit parameter sets a and b is calculated as

$$C_{ab} = \frac{1}{N-1}\frac{\sum_{i=1}^{N}(a_i-\mu_a)(b_i-\mu_b)}{\sigma_a\sigma_b} \quad (1)$$

where a_i and b_i are the ith results of the ordered set of fit parameter results. $\mu_{a,b}$ and $\sigma_{a,b}$ are the arithmetic means and the standard deviations of sets a and b, respectively.

Parameters for each subsequent MC run can be initialized by either using the results of the previous iteration or using new random values. Seeding each fit with a new random set significantly increases the time required for searching parameter space, but is a powerful means of assessing whether the obtained nSLD profile corresponds to the global minimum within a chosen model. In this work, MC iterations were seeded with random values.

In addition to determining objective measures for parameter confidence, MC output also provides a convenient tool for visualizing the variational bandwidth associated with the nSLD profile due to data scatter. By mapping each nSLD profile generated in the MC resampling onto an ρ_n–z grid with a constant bin size, a 2D matrix is generated whose element values contain the frequency by which this element is occupied by any of the nSLD curves. This matrix may then be used to visualize $\rho_n(z)$ and the associated probabilities of deviations from the best-fit profile. Such plots are handy tools in determining which regions in the nSLD profiles are well defined.

All of the capabilities described above have been implemented in a wrapper script in the most recent version of ga_refl.[28]

III. Results

Self-Assembled Monolayers. Mixed SAM formation was investigated over a range of FC16/βME ratios from 100:0 to 10:90 and over a range of immersion times from 4 h to 3 days. Whereas it is anticipated that the larger FC16 may exhibit a slightly larger propensity to adsorb to Au relative to βME, we do not expect the surface-bound concentrations χ_{FC16} and $\chi_{\beta ME}$ to be substantially different from the solution concentration. Therefore, FC16/βME ratios throughout this article are quoted as concentrations in the adsorption solution.

Whereas the SAMs formed quickly from solution to a completion of ~90% (within approximately 1 min for WC14, ref 10), full coverage of the surface require longer immersion times. We assessed the surface properties in terms of static contact angles (θ) and spectroscopic ellipsometric thickness d_{SE} estimates of the surface films after 4 h and 1 and 3 days of immersion (Figure 1 and Table 1). The FC16/βME SAMs consistently had high contact angles and constant organic thicknesses from 100% FC16 up to βME molar ratios of 50%. Upon increasing the βME concentration further, d_{SE} decayed linearly to the value for pure βME whereas θ decreased from >105° to a plateau near 80°, which persisted to a βME molar ratio of 90%, which is significantly larger than the low hydrophobicity of an interface modified by pure βME ($\theta_{\beta ME} \approx 30°$).

Figure 1 illustrates the behavior of d_{SE} and compares the FC14/βME results with those obtained for WC14/βME in earlier work.[10] Consistent with expectations based on the structural differences of FC16 and WC14, FC16/βME SAMs had larger thicknesses throughout the entire range of backfiller concentrations. As expected, these differences are more pronounced at high concentrations of the membrane anchors. Importantly, the regime of FC16 concentrations at which we observed the full thickness of the organic layer, $d_{SE} \approx 40$ Å, extends down to 50 mol %, which is significantly lower than that observed with WC14/βME = 80:20. This indicates that the longer alkyl chain increases the

(25) Lu, J. R.; Thomas, R. K.; Penfold, J. *Adv. Colloid Interface Sci.* **2000**, *84*, 143–304.
(26) Vacklin, H. P.; Tiberg, F.; Fragneto, G.; Thomas, R. K. *Langmuir* **2005**, *21*, 2827–2837.
(27) Dura, J. A.; Pierce, D.; Majkrzak, C. F.; Maliszewskyj, N.; McGillivray, D. J.; Lösche, M.; O'Donovan, K. V.; Mihailescu, M.; Perez-Salas, U. A.; Worcester, D. L.; White, S. H. *Rev. Sci. Instrum.* **2006**, *77*, 074301.
(28) Kienzle, P. A.; Doucet, M.; McGillivray, D. J.; O'Donovan, K. V.; Berk, N. F.; Majkrzak, C. F. *ga_refl*, 2000−2009.
(29) Parratt, L. G. *Phys. Rev.* **1954**, *95*, 359–369.
(30) Press, W. H.; Flannery, B. P.; Teukolsky, S. A.; Vetterling, W. T. *Numerical Recipes*; Cambridge University Press: Cambridge, U.K., 1986.
(31) Vaknin, D.; Kjaer, K.; Als-Nielsen, J.; Lösche, M. *Biophys. J.* **1991**, *59*, 1325–1332.

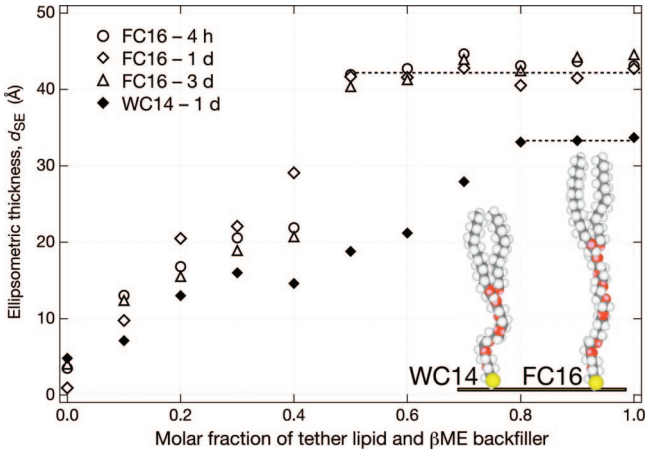

Figure 1. Ellipsometric thickness of SAMs based upon FC16 or WC14 (data from ref 10) as a function of tether spacing by increasing the amount of βME in the adsorption solution. Dashed lines are guides for the eye. (Inset) Molecular structure of the two membrane anchors.

Table 1. Ellipsometric Thicknesses, d_{SE}, and Contact Angles, θ, of FC16/βME SAMs as a Function of the FC16/βME mol % Ratio in the Adsorption Solutions[a]

fraction of FC16/mol%	ellipsometric thickness/Å (4 h of immersion)	contact angle/deg
0	3.5 ± 0.3	33 ± 5
10	13.0 ± 0.2	75 ± 3
20	16.8 ± 0.4	82 ± 3
30	20.6 ± 0.3	82 ± 3
40	21.9 ± 0.4	87 ± 3
50	41.9 ± 0.4	106 ± 2
60	42.7 ± 0.4	106 ± 1
70	44.7 ± 0.4	106 ± 2
80	43.1 ± 0.4	106 ± 1
90	43.6 ± 0.4	107 ± 2
100	43.1 ± 0.4	109 ± 1

[a] Uncertainties in d_{SE} reflect variabilities of measurement across one wafer. The ellipsometric thicknesses of different preparations (wafers) may vary more than the quoted uncertainties. Uncertainties in θ are standard deviations of typically four measurements per sample.

molecular order through enhanced van der Waals interactions. The differences in d_{SE} at high lipid anchor concentrations (~40 Å for FC16 vs ~30 Å for WC14) are consistent with the different molecular structures. For FC16/βME, however, no significant differences in d_{SE} were observed for immersion times >4 h (Figure 1), suggesting that prolonged immersion does not increase molecular order further.

Figure 2 shows the FT-IRRAS features of pure FC16 SAMs in the C−H stretching region from 3500 to 2500 cm^{-1} and the midrange from 1400 to 800 cm^{-1}. The prominent band at 1132 cm^{-1}, assigned as the C−O and C−C stretching bands, and irregular baseline in the midrange region indicate a disordered NEO segment[32] that should be able to incorporate water in the presence of an aqueous environment. Absent in this region are any spectral features of helical[33] or all-trans[34] conformational order in the EO segment. The IR data suggests no order over any significant segment of the NEO chain. The C−H region is also largely featureless because of the overlap of the methylene stretching bands of the NEO segment and the methyl and

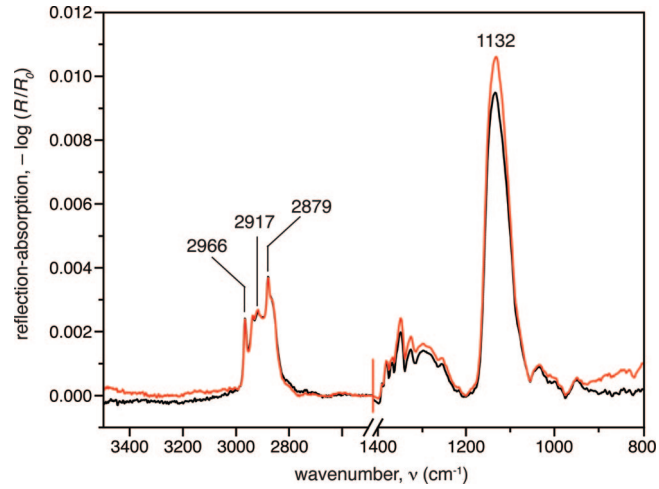

Figure 2. Two independently measured FT-IRRA spectra of 100% FC16 SAMs.

methylene stretching bands of the hexadecyl chains. Discernible bands at 2966, 2917, and 2879 cm^{-1} are assigned as the ν_a (ip) (CH_3), ν_{as} (CH_2), and ν_s (FR) (CH_3) modes, respectively.[35] The absorption band at 2917 cm^{-1} suggests order in the alkyl chains, which is consistent with the earlier FT-IRRAS data on WC14 and the increased SE thickness data.

Sparsely Tethered Bilayer Lipid Membranes: Zwitterionic Lipids. Bilayers were formed from the precursor SAMs by rapid solvent exchange.[10] We studied stBLMs completed with DPhyPC extensively in EIS measurements to compare the capability of FC16 to serve as the basis for fluid, tightly sealing membranes with that of WC14. DPhyPC-containing stBLMs at FC16/βME = 30:70 and 15:85 were structurally characterized with NR. Because success in the formation of WC14-based stBLMs containing anionic phospholipids has been variable in our hands, we also investigated a set of FC16-based samples formed from zwitterionic/anionic lipid mixtures.

Electrochemical Impedance Spectroscopy. Figure 3A shows a series of EI spectra of FC16-based stBLMs with different FC16/βME from 100:0 to 10:90, completed with DPhyPC. The Cole−Cole plots show a systematic progression from spectra that consist of semicircles with small radii (corresponding to bilayer capacitances of ~0.6 μF/cm^2 for 100−50 mol % FC16) to subsequently larger semicircles (larger capacitances) that show low-frequency tails with increasing lengths. In earlier work,[9] we argued that the length of the tail is associated with the defect density of the stBLMs.

The inset in Figure 3A shows the equivalent circuit model (ECM) used to determine the electrical characteristics of the stBLMs quantitatively. It uses constant-phase elements (CPEs) with an impedance defined as

$$Z_{CPE} = \frac{1}{CPE(i\omega)^{\alpha}} \quad (2)$$

to account for imperfections of the membrane, such as surface roughness with an empirically determined dependence on cyclic frequency, ω. As $\alpha \rightarrow 1$, this impedance is that of the capacitance of an ideal membrane, $C_{membrane}$. The CPE in the defect branch originates from in-plane components of the electrical field surrounding a defect. This in-plane component decays with distance from the defect center and couples to the Helmholtz capacitance of the interface between the Au electrode and the

(32) Dissanayake, M. A. K.; Frech, R. *Macromolecules* **1995**, *28*, 5312–5319.
(33) Vanderah, D. J.; Meuse, C. W.; Silin, V.; Plant, A. L. *Langmuir* **1998**, *14*, 6916–6923.
(34) Harder, P.; Grunze, M.; Dahint, R.; Whitesides, G. M.; Laibinis, P. E. *J. Phys. Chem. B* **1998**, *102*, 426–436.
(35) Hussain, H.; Kerth, A.; Blume, A.; Kressler, J. *J. Phys. Chem. B* **2004**, *108*, 9962–9969.

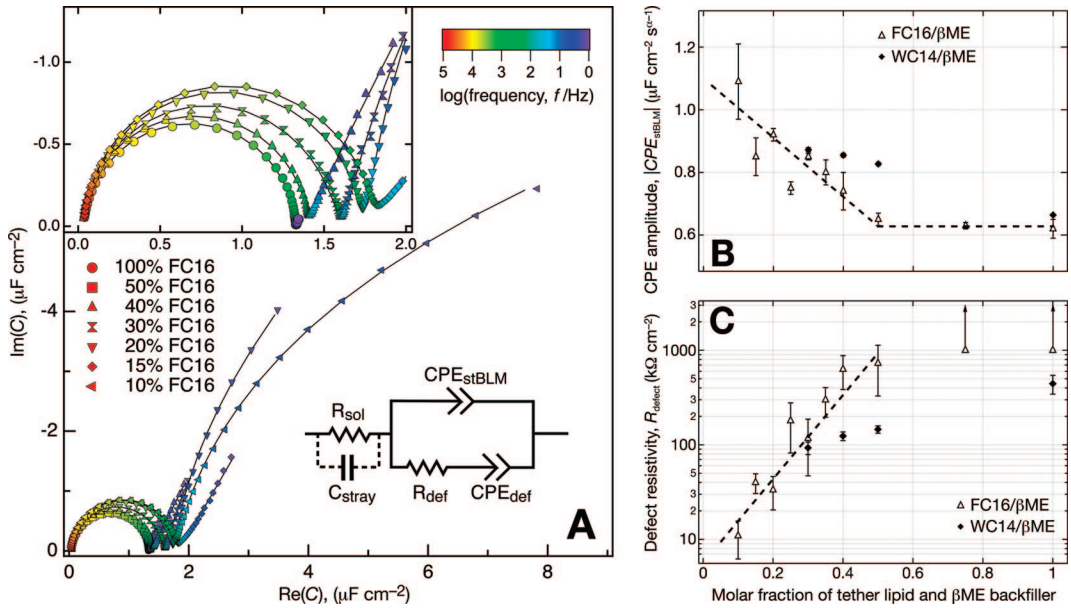

Figure 3. EIS data of stBLMs completed with DPhyPC and derived electrical parameters. (A) The main panel and upper left inset show Cole−Cole plots of FC16-based stBLMs. Seven data sets with βME backfiller ratios as indicated are plotted in the main panel, where the length of the low-frequency tails correlates with the defect density in the bilayer.[10] In the inset, data sets for FC16/βME = 10:90 and 50:50 have been omitted for clarity. The ECM used to model the data is shown in the lower right. (B, C) Membrane CPE amplitudes (approximately equivalent to membrane capacitances) and defect resistivities of FC16-based stBLMs derived from data such as those shown in plot A by fitting to the ECM. Corresponding results for WC14-based stBLMs (data from ref 10) could not be determined at comparably low tether densities as for FC16. Dashed lines are guides for the eye.

Table 2. Best-Fit Parameters for EI Spectra of stBLMs Completed with DPhyPC[a]

fraction of FC16/mol%	100	75	50	40	35	30	25	20	15	10
CPE_{stBLM}/ $\mu F\ cm^{-2}\ s^{(\alpha-1)}$	0.62 ± 0.03	0.63 ± 0.01	0.65 ± 0.02	0.74 ± 0.06	0.80 ± 0.04	0.85 ± 0.01	0.75 ± 0.02	0.92 ± 0.02	0.85 ± 0.06	1.09 ± 0.12
α_{stBLM}	0.997 ± 0.001	0.998 ± 0.001	0.996 ± 0.001	0.991 ± 0.003	0.994 ± 0.003	0.991 ± 0.005	0.995 ± 0.002	0.989 ± 0.002	0.991 ± 0.003	0.972 ± 0.015
CPE_{defect}/ $\mu F\ cm^{-2}\ s^{(\alpha-1)}$	n/a	n/a	0.92 ± 0.42	4.22 ± 1.77	1.07 ± 0.29	3.81 ± 0.59	2.48 ± 1.10	8.54 ± 0.96	4.65 ± 0.80	10.1 ± 1.2
α_{defect}	n/a	n/a	0.521 ± 0.077	0.442 ± 0.059	0.501 ± 0.057	0.459 ± 0.105	0.417 ± 0.039	0.601 ± 0.111	0.382 ± 0.096	0.741 ± 0.033
R_{defect}/kΩ cm^2	>1000	>1000	731 ± 402	631 ± 246	299 ± 103	117 ± 70	180 ± 98	33.4 ± 12.9	40.0 ± 9.4	10.9 ± 4.7
fit quality/10^{-5}	1.84	1.16	1.52	2.23	2.91	3.52	1.83	3.22	1.23	6.25

[a] Varying FC16/βME from 100:0 to 10:90 was used for the preparation of the parent SAM in the immersion solution. Averages were derived from at least three independent samples.

submembrane space. The components in the dotted branch of the ECM account for the conductivity of the bulk electrolyte and stray capacitances associated with the sample cell and cables.

In fitting the data with the ECM (Figure 3A), we noticed that the resistance of the defect branch at high FC16 ratios was so large that it could not be reliably determined. (Note that the low-frequency tails in the Cole−Cole plots that are well developed for samples with high backfiller concentrations vanish for FC16/βME > 50:50). The parameters that describe the defect branch are then ill-defined. Our approach was to fix α_{defect} at 0.5, which yielded R_{defect} values in the 3 MΩ cm^2 range, to determine CPE_{stBLM}. Foregoing the defect branch in the ECM altogether yielded very similar results for CPE_{stBLM} and α_{stBLM}. Figure 3B shows the development of the CPE amplitude and defect resistance R_{defect} as a function of anchor/backfiller composition in which FC16-based stBLMs are compared with WC14-based stBLMs. Again consistent with expectations based on the differences in molecular structures between the two anchor molecules, FC16-based bilayers tend to have larger resistances and lower capacitances ($C \approx |CPE|$ because $\alpha \approx 1$). Table 2 shows the fitting results in detail.

Neutron Reflection. The backfiller concentration range in which we are most interested is at large proportions of βME, where anchoring points of the membrane are well diluted and their interference with in-plane bilayer dynamics can be expected to be minimized. In earlier studies of WC14, we observed that structurally well-defined and functionally intact, tightly sealed membranes were obtained for WC14/βME ratios down to ~30:70. All results discussed so far indicated that FC16/βME forms well-defined membranes at even lower anchor densities. We therefore characterized FC16/βME-based stBLMs with NR at 30:70 and at 15:85 in order to obtain a direct comparison with WC14 and to provide a reference system for the utilization of FC16 at even lower concentration in future work.

Figure 4A shows representative NR results for an stBLM of FC16/βME = 30:70. Data have been normalized by the Fresnel reflectivity, R_F. The bilayer was completed with DPhyPC in D_2O, and the NR spectrum was measured. The buffer phase was then exchanged in situ for an H_2O/D_2O mixture with a neutron scattering length density (nSLD) of $\rho_n = 4 \times 10^{-6}$ $Å^{-2}$ (CM4) where the NR was measured, and finally, the buffer phase was again exchanged for H_2O and the NR was determined. A simultaneous fit to all three data sets was performed with a slab model that included three layers for the surface of the inorganic substrate [(1) SiO_x, (2) Cr, and (3) Au] and four layers for the stBLM structure [(4) thiol/βME/hydrated tether/inner lipid headgroups, (5) inner alkane layer, (6) outer alkane layer, and (7) outer phospholipid headgroups]. The results, and those from a similar set of measurements on an stBLM with FC16/βME = 15:85 (data not shown), are summarized in Table 3, and the

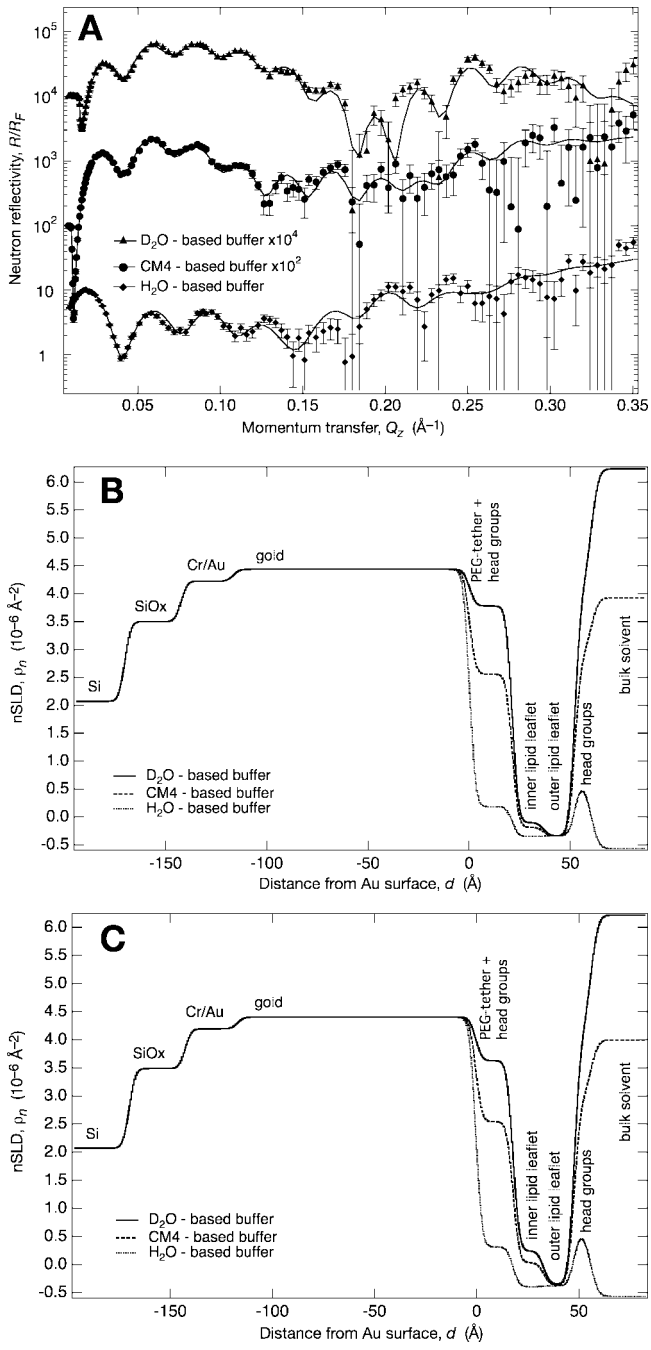

Figure 4. NR data and resulting nSLD profiles for FC16-based stBLMs completed with DPhyPC. (A, B) Data and nSLD profiles for FC16/βME = 30:70. (C) nSLD profiles for FC16/βME = 15:85. The neutron reflection data in panel A have been normalized by the reflectivity of the idealized Si/buffer interface (i.e., the Fresnel reflectivity R_F). This representation better shows the interference pattern, particularly at high momentum transfer.

corresponding nSLD profiles are shown in Figure 4B,C. The Table also contains results for stBLMs completed with mixtures of zwitterionic and anionic phospholipids, POPC and POPG (see below).

The fact that all neutron data sets determined for isotopically contrasted samples can be well described by nSLD profiles derived from one unique model indicates that these stBLMs form laterally homogeneous bilayer structures. A close inspection of Figure 4 shows that the profiles are consistent with structures in which the membrane is decoupled from the inorganic substrate by a nanometer-thick hydration layer. The solvent contents of the four distinct organic layers in each stBLM can be directly assessed from the model because of their characteristic differences in nSLD as a function of the isotopic composition of the aqueous phases. This analysis shows that the water content in the ~20-Å-thick submembrane layer is on the order of 50 vol %. The alkane layers that form the hydrophobic cores of the membrane are essentially water-free. In the stBLMs formed on FC16/βME = 30:70, the monolayer proximal to the substrate is essentially free of solvent (4% ± 3%). At 15:85, this monolayer contains some solvent, indicating that the inner leaflet is no longer completely reconstituted with phospholipid in the rapid solvent exchange at this higher dilution of the membrane anchor. The distal monolayer leaflets are defect-free and show no indication of solvent inclusion in any of the samples. The PC headgroups are clearly recognized as regions of elevated nSLD at distances of ~50 Å from the Au film in the profiles measured with H_2O solvent. In earlier NR measurements of Langmuir monolayers composed of DPPC, we determined the nSLD of the PC headgroup, $\rho_n^{PC} = 1.8 \times 10^{-6}$ Å^{-2}.[31] To reduce the number of model parameters, we fixed their thickness generally at $d = 7$ Å, its approximate value,[31] and constrained the nSLD of the slab such that the headgroups appeared to be well hydrated in the model (50 vol % water content). This value is close to the values typically observed for stBLMs based upon WC14 membrane anchors.[10] Figure 5 shows parameter distributions (tether layer thicknesses and hydrophobic chain monolayer thicknesses for stBLMs of the two distinct SAM compositions, Figure 5A) determined by MC resampling of the data that indicate that the extension of the tethers and the hydrophobic membrane slab thickness both shrink as the lateral tether density is reduced. Not only are the NR measurements precise enough to measure these differences but the MC resampling also shows that these differences are indeed significant.

Sparsely Tethered Bilayer Lipid Membranes: Zwitterionic/Anionic Lipid Mixtures. We also investigated stBLMs formed on SAMs of FC16/βME = 30:70 using charged phospholipids. In earlier work with WC14, attempts to complete bilayers entirely with anionic phospholipids failed in that the resulting bilayers were often incomplete, and stBLMs formed from anionic/zwitterionic mixtures were also defect-rich with substantial water content in the hydrophobic membrane slabs (Heinrich and McGillivray, unpublished results). Here we tested mixtures of POPC and POPG (80:20) for their capacity to form structurally well-defined stBLMs on the basis of FC16 membrane tethers. Because it is likely that the relative amounts of POPC and POPG in the stBLM differ from that in the solution used to complete the bilayer and it is difficult to determine the stoichiometry of the lipids at the surface experimentally, we investigated two samples of different isotopic compositions. One sample was composed entirely of hydrogenated phospholipids whereas the second sample incorporated hydrogenated POPC and POPG on which the palmitoyl chain was perdeuterated (d_{31}-POPG).

Structural Analysis (Neutron Reflection). The NR data (not shown) were modeled with an approach similar to that described for DPhyPC stBLMs and yielded nSLD profiles that were consistent with the formation of well-defined and laterally homogeneous and complete bilayer structures (Figure 6A,B). A comparison of the fully hydrogenated and the partially deuterated sample shows that the preparation is reasonably reproducible in its geometric structure. Model parameters are also summarized in Table 3 for comparison with those of the zwitterionic stBLMs. As realized from the nSLD profiles and borne out in the Table, the bilayers are indeed 100% complete and generally similar to the stBLMs completed with DPhyPC. Remarkably, however,

Table 3. Best-Fit NR Models of the Investigated stBLMs

parameter	FC16/βME = 30:70; DPhyPC	FC16/βME = 15:85; DPhyPC	FC16/βME = 30:70; POPC/POPG = 80:20	FC16/βME = 30:70; *h*-POPC/*d*-POPG = 80:20
		Layer Thicknesses/Å		
d_{SiO_x}	27.6 ± 1.1	27.5 ± 1.4	29.9 ± 1.8	37.3 ± 1.6
d_{Cr}	25.8 ± 1.9	25.8 ± 2.3	23.6 ± 2.5	13.6 ± 3.1
d_{Au}	116.9 ± 1.7	116.5 ± 2.6	124.4 ± 1.7	122.6 ± 2.1
d_{tether}	21.1 ± 0.7	18.3 ± 0.9	15.4 ± 0.7	17.2 ± 1.4
$d_{lipid\ chains}$	15.5 ± 0.3	14.9 ± 0.4	12.7 ± 0.4	13.2 ± 0.7
$d_{outer\ lipid\ headgroup}$		7 (fixed)		
		Neutron Scattering Length Densities/10^{-6} Å^{-2}		
$\rho_n^{SiO_x}$	3.50 ± 0.05	3.49 ± 0.06	3.4 (fixed)	3.4 (fixed)
ρ_n^{Cr}	4.22 ± 0.04	4.19 ± 0.05	4.0 (fixed)	4.0 (fixed)
ρ_n^{Au}	4.44 ± 0.02	4.40 ± 0.02	4.40 ± 0.01	4.37 ± 0.01
ρ_n^{tether}	1.07 ± 0.17	1.15 ± 0.19	1.0 (fixed)	1.0 (fixed)
$\rho_n^{inner\ lipid\ chains}$	−0.36 ± 0.05	−0.38 ± 0.06	−0.31 ± 0.05	−0.49 ± 0.15
$\rho_n^{outer\ lipid\ chains}$				+0.60 ± 0.10
$\rho_n^{outer\ lipid\ headgroup}$		1.79 (fixed)		
		Volume Fractions of Layer Content		
water vf_{tether}	0.53 ± 0.02	0.49 ± 0.03	0.18 ± 0.03	0.23 ± 0.03
alkane $vf_{inner\ lipid\ ch}$	0.96 ± 0.03	0.91 ± 0.04	1.00 ± 0.01	1.00 ± 0.01
alkane $vf_{outer\ lipid\ ch}$	1.00 ± 0.01	1.00 ± 0.03	1.00 ± 0.01	1.00 ± 0.01
water $vf_{outer\ lipid\ hg}$		0.50 (fixed)		
		Roughness/Å		
σ	5.8 ± 0.6	5.8 ± 1.0	5.0 ± 0.9	5.0 ± 0.2
χ^2	3.32	2.74	2.33	2.86

the thickness of the tether slab is marginally, but significantly, smaller than that observed with the zwitterionic phospholipid at the same FC16/βME = 30:70. Accordingly, the hydration of the submembrane space is somewhat lower in the charged samples than for the zwitterionic lipids (Figure 5B), possibly because of the attraction of the charged headgroups to the interface by image charges. Also, we observe a slightly reduced thickness of the hydrophobic membrane slabs, which reflects the higher intrinsic disorder of the unsaturated chains in comparison with the phytanoyl chains.

Combining the NR results for the fully hydrogenated sample with that for the sample in which POPG was deuterated on the *sn*-1 chain (Table 3, columns 3 and 4, respectively) allows an estimate of the proportions of PC and PG in the stBLM by virtue of the increase in nSLD in the distal lipid chain leaflet. Using the result for the fully hydrogenated sample ($\rho_n^{chain} = -0.31 \times 10^{-6}$ Å^{-2}), we calculate an average area per lipid of the POPC/POPG mixture of $A = 68 \pm 7$ Å^2. In the sample formed with *d*-POPG, the proximal leaflet is devoid of the deuterated label, indicating that the charged lipid remains entirely in the distal monolayer. From the observed nSLD of this layer, we estimate that the proportion of *d*-POPG in the mixture is 20 ± 5%.

Parameter Confidence Limits and Parameter Coupling. Given the general structure of the data, in which the pattern of interference minima appears to be strongly dominated by the structural features of the high-index Au film, it is particularly interesting to determine to what extent the structural parameters of the (mostly) low-index organic film features depend on the parameters of the Au film. The MC resampling procedure is also useful in assessing correlations between the model parameters. Table 4 shows the covariance matrices for both POPC/POPG data sets. Correlations directly reflect the width of the parameter distributions and therefore the size of the confidence interval given in Table 3, as illustrated in Figure 7. The analysis reveals strong correlations between the layer properties of the SiO_x, Cr, and Au films. Correlations between the Au film and the organic overlayers are not nearly as strong. In particular, the correlations between the Au and Cr film structure (Figure 7A) suggest inadequacies in the model for the chemically complex Cr bonding layer and indicate the interdiffusion of Au atoms into the Cr layer, resulting in an nSLD that is much larger than that for pure Cr (and/or a larger roughness of the Cr/Au interface). We chose to model the Cr layer with an nSLD that is substantially higher than that expected for pure Cr ($\rho_n^{Cr} \approx 3 \times 10^{-6}$ Å^{-2}) and use a roughness parameter, σ, identical to the roughness of all other interfaces (global roughness approach).

Strong correlations are also observed between the proximal lipid leaflet and the tethered layer (Figure 7B), possibly derived from an oversimplification in modeling the chemically complex tether region whereas the correlation between the Au film and the organic layers is weak (Figure 7C,D). There is no evidence that the "domination" of the NR spectrum by the Au film impairs the determination of the structure of the stBLM. In both cases where correlations are high, those occur in a very narrow (confidence) interval, so the affected parameters can still be determined to high precision. For example, substrate layer thicknesses are typically determined from NR data to ±3 Å, and the thicknesses of layers in the stratified organic surface architecture are determined to ±1 Å. A probability plot for the nSLD profiles of the 80:20 mol/mol POPC/*d*-POPG stBLM in D_2O derived from the MC resampling (Figure 8) illustrates this point impressively. This depiction shows the implications of parameter coupling and that the main range of uncertainty in the nSLD profiles is located at the Cr/Au interface and does not transcend the organic surface architecture, as is realized by the observation of a sharp interface between the Au film and the tethered layer.

IV. Discussion

Similar to WC14-anchored bilayers, FC16-based stBLMs are highly insulating on SAMs without βME or at low backfiller concentrations. However, tBLMs without backfiller do not contain solvent in the submembrane layer, typically <5 vol %,[10] and are not particularly well suited to membrane protein incorporation (McGillivray et al., unpublished results). Backfilling results in the lateral dilution of membrane anchors and renders the stBLM amenable to the reconstitution of proteins, such as α-hemolysin (αHL).[13] As shown earlier, there is a limit to the dilution of the membrane anchor in the SAMs at which hydrophobic chains do not attain an upright orientation on the Au surface. Although rapid solvent exchange may still lead to the formation of well-ordered bilayer structures, such stBLMs show progressively

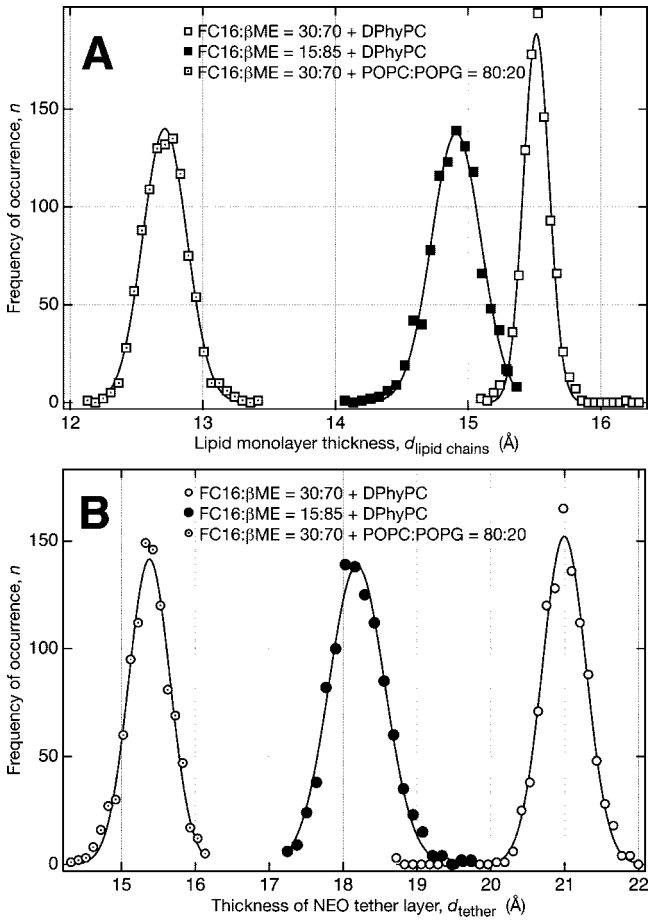

Figure 5. Histograms of best-fit parameter values for layer thicknesses in the slab models that describe the NR data from FC16-based stBLMs.

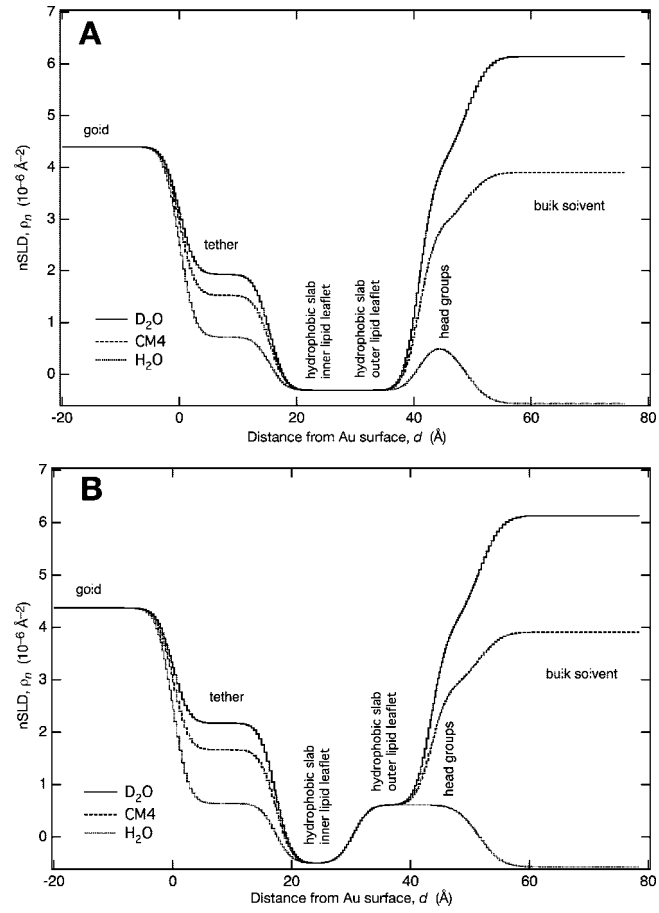

Figure 6. Neutron scattering length density profiles for FC16-based stBLMs (FC16/βME = 30:70) completed with POPC/POPG (80:20) in the solution used in the rapid solvent exchange. (A) Both phospholipid species were hydrogenated. (B) POPC/*d*-POPG. The inorganic substrate is not shown in this view but is similar to the one shown in Figure 4B,C.

poorer electrical resistance with increasing proportions of βME. We reasoned that an extension of the polymethylene chains onto the membrane anchor might promote the formation of stBLMs in which the anchor density could be further reduced. Importantly, the increased tether length may increase the thickness of the submembrane space and the flexibility of the anchored lipid, thereby potentially offsetting reductions in membrane fluidity that might arise from the increase in dispersion interactions.

All of the results presented here bear out these expectations, although the differences between FC16-based and WC14-based stBLMs, particularly in their electrical parameters, are rather moderate. Nevertheless, all structural and functional metrics indicate that stBLMs are well organized at lower tether densities with FC16 than with WC14. Moreover, as judged from our initial attempt, mixed membranes containing anionic phospholipids form more readily on FC16-based SAMs than on WC14.

In structural terms, the bilayers formed on FC16 are extremely well defined. Down to FC16/βME = 25:75, the bilayers are virtually defect-free by NR and EIS data. Only at FC16/βME = 15:85 does NR start to show water-filled defects in the hydrophobic bilayer core by virtue of isotopic contrast variation of the aqueous buffer. The thickness of the submembrane space is slightly larger with FC16 than with WC14 (~20 vs ~15 Å). As with WC14, it is thinner than the extended length of the oligo(ethylene oxide) spacer, consistent with the IR results indicating disordered oligo(ethylene oxide) chains. The submembrane layer is highly hydrated, particularly at high dilution of the membrane anchor (≥50% water by volume).

As estimated from the observed nSLD of the hydrophobic membrane interior, the lateral area per phospholipid within the bilayers is $A \approx 70$ Å^2 (POPC/POPG), a value that is comparable to that reported for fully hydrated POPC multibilayer membranes,[36] and $A \approx 75$ Å^2 (DPhyPC), which is slightly less than the value estimated from X-ray scattering.[37] From these results, one would expect that the mobility of phospholipids in the stBLMs should be comparable to that in free lipid bilayers, at least in the monolayer leaflet distal with respect to the inorganic substrate. Diffusion measurements using fluorescence correlation spectroscopy (FCS) of labeled phospholipids in such stBLMs indicate that the mobility is indeed somewhat reduced but of the same order of magnitude (Moldovan, Shenoy, and Lösche, preliminary results).

The notion that the proximal and distal monolayer sheets may be distinctly different in the stBLMs is borne out in the NR experiments with palmitoyl-perdeuterated POPG. The results indicate that *d*-POPG partitions entirely into the distal monolayer where the PC/PG ratio is approximately the same as in the immersion solution used for rapid solvent exchange. In fact, the apparent nSLD drop in the proximal chain monolayer from the value observed in fully hydrogenated phospholipid (POPC/POPG) to that of the hydrogenated/deuterated mixture (POPC/

(36) Kucerka, N.; Liu, Y. F.; Chu, N.; Petrache, H. I.; Tristram-Nagle, S.; Nagle, J. F. *Biophys. J.* **2005**, *88*, 2626–2637.
(37) Wu, Y.; He, K.; Ludtke, S. J.; Huang, H. W. *Biophys. J.* **1995**, *68*, 2361–2369.

Table 4. Covariance Matrices of the Best-Fit Model Parameters for the NR Data Sets from FC16-Based (FC16/βME = 30:70) stBLMs Completed with 80:20 *h*-POPC/*d*-POPG (Lower Left Triangle) and 80:20 *h*-POPC/*h*-POPG (Upper Right Triangle)

	d_{SiO_x}	d_{Cr}	d_{Au}	d_{tether}	$d_{lipid\ chains}$	vf_{tether}	$vf_{inner\ lipid\ ch}$	$vf_{outer\ lipid\ ch}$	ρ_n^{Au}	$\rho_n^{inner\ lipid\ ch}$	$\rho_n^{outer\ lipid\ ch}$	$\rho_n^{D_2O}$	ρ_n^{CM4}	σ
d_{SiOx}		−0.72	0.20	−0.25	0.15	0.17	0.04	−0.05	0.21	0.20		−0.03	−0.04	−0.21
d_{Cr}	−0.86		−0.80	0.19	−0.05	−0.19	0.00	0.01	0.12	−0.11		0.02	0.01	0.16
d_{Au}	0.64	−0.93		−0.10	−0.08	0.20	−0.02	0.01	−0.36	−0.02		−0.01	0.02	−0.01
d_{tether}	−0.09	0.15	−0.23		−0.84	0.26	0.05	0.06	−0.11	−0.74		−0.05	−0.01	0.23
$d_{lipid\ chains}$	0.02	−0.06	0.09	−0.93		−0.65	−0.05	−0.07	0.17	0.84		0.09	0.08	−0.39
vf_{tether}	0.20	−0.20	0.20	0.54	−0.77		0.01	0.01	−0.06	−0.36		−0.18	−0.11	0.25
$vf_{inner\ lipid\ ch}$	−0.06	0.11	−0.14	0.33	−0.27	0.05		−0.05	0.02	−0.02		−0.01	−0.01	0.06
$vf_{outer\ lipid\ ch}$	0.00	−0.01	0.00	0.01	0.00	−0.03	0.05		−0.04	−0.07		0.01	−0.01	0.10
ρ_n^{Au}	0.02	0.18	−0.35	0.17	−0.04	−0.12	0.08	−0.04		0.26		0.24	−0.02	−0.08
$\rho_n^{inner\ lipid\ ch}$	0.16	−0.19	0.19	−0.81	0.80	−0.50	−0.10	−0.01	−0.07			0.12	0.01	−0.49
$\rho_n^{outer\ lipid\ ch}$	−0.14	0.18	−0.20	0.54	−0.43	0.24	0.31	0.02	0.20	−0.70				
$\rho_n^{D_2O}$	−0.05	0.08	−0.10	0.05	−0.02	−0.12	−0.08	−0.01	0.23	0.00	0.03		−0.04	−0.01
ρ_n^{CM4}	−0.06	0.03	0.01	−0.05	0.10	−0.14	0.00	0.10	−0.09	0.05	−0.07	−0.03		−0.02
σ	−0.01	−0.02	0.03	−0.06	0.07	−0.08	0.00	0.08	−0.03	0.01	−0.02	−0.03	0.03	

d-POPG) suggests that the deuterated compound is quantitatively excluded from the proximal leaflet. One might have expected that the nominal nSLD values of the membrane interior in the POPC/POPG stBLM and of the proximal leaflet in the POPC/*d*-POPG stBLM should be identical. However, even while the precision of the nSLD value in the latter case is reduced, we note that there may be, in fact, differences in the average densities of the proximal and distal layers due to the distinct chain ligations in phospholipids (acyl chains) and in the membrane anchor (alkyl chains). Because the alkyl chains can pack more densely, the proximal layer may have a higher density than the distal layer. For fully hydrogenated lipids, we cannot discriminate in the NR model between those monolayers. The nSLD values observed there may represent an average of two different densities.

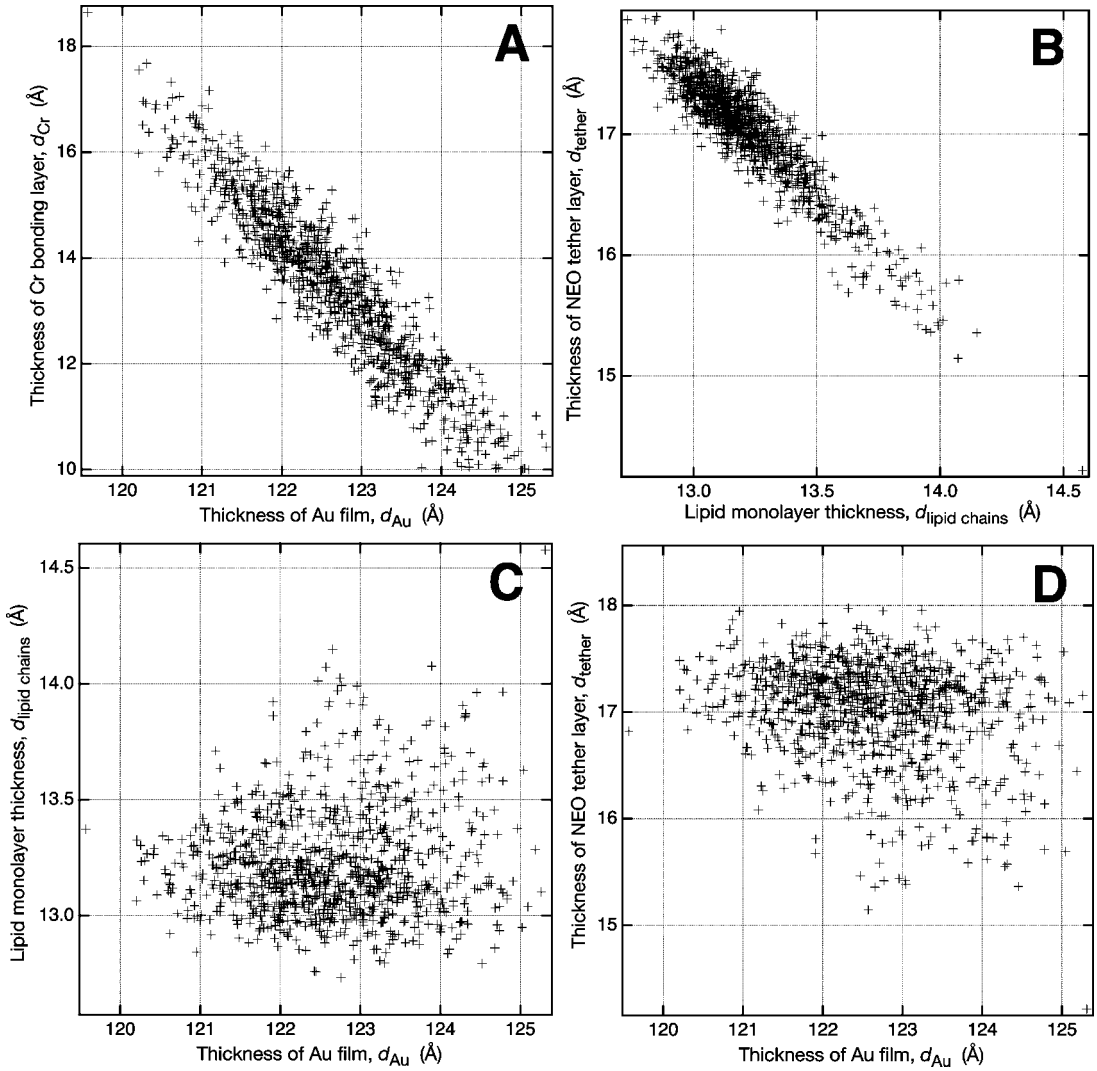

Figure 7. Exemplary visualization of parameter correlations (Table 4) in the modeling of NR spectra by Monte Carlo resampling of the data. For the FC16-based stBLM (FC16/βME = 30:70) completed with POPC/*d*-POPG (80:20) in the solution used for rapid solvent exchange, these plots show the distribution of parameter pairs in the best-fit models that describe resampled virtual data sets. (A) d_{Au} vs d_{Cr}; covariance coefficient, $\eta = -0.93$. (B) $d_{lipid\ chains}$ vs d_{tether}; $\eta = -0.93$. (C) d_{Au} vs $d_{lipid\ chains}$; $\eta = 0.09$. (D) d_{Au} vs d_{tether}; $\eta = -0.23$.

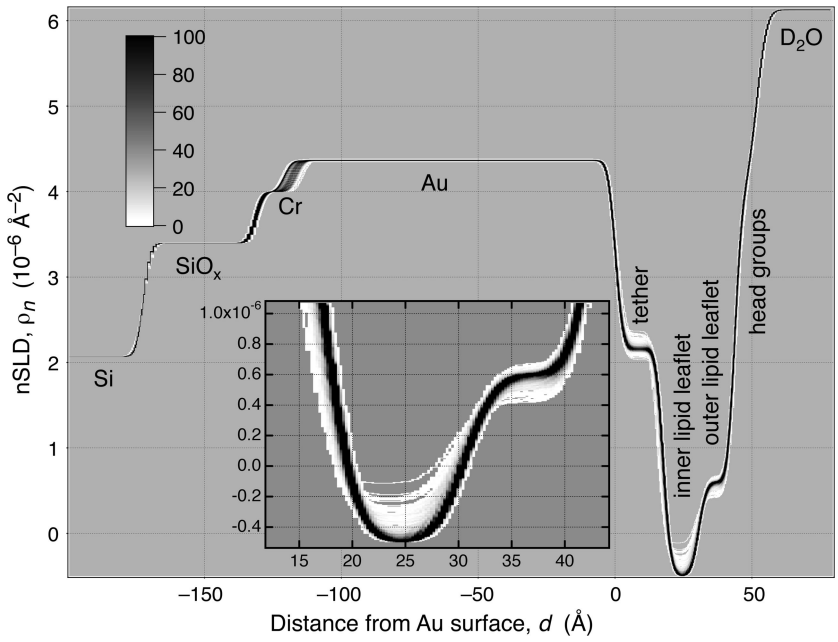

Figure 8. Result from the MC resampling of NR data. A probability plot (FC16/βME = 30:70 stBLM completed with POPC/*d*-POPG = 80:20) shows a superposition of all nSLD profiles in which shades of gray show the frequency by which a grid point is hit. Black codes for 100 or more of a total of 1000 occurrences. This view gives a visual impression of how well certain regions in the surface architecture are determined by the NR data sets.

In the limited range of lipids that we have used to form stBLMs based upon FC16, we observed consistently that the submembrane space in partially charged bilayers is slightly reduced from the values observed for fully zwitterionic bilayers. This leads us to the interesting hypothesis, to be tested in future work, that electrostatic forces increase the attraction of charged headgroups to the conducting Au film and lead to a reduction in equilibrium distance of the bilayer from the surface.

V. Conclusions

We investigated and compared quantitatively the structural and functional properties of stBLMs based upon two different membrane lipid anchors backfilled with βME. FC16, which comprises longer polymethylene chains (dipalmityl) and a longer hydrophilic oligo(ethylene oxide) tether (nine ethylene oxide units) than WC14 (dimyristyl and six ethylene oxide units), forms bilayers that show increased resistivity to ion transfer. The submembrane space is ~0.5 nm wider for FC16-based stBLMs than for WC14-based stBLMs. stBLMs that include charged phospholipids comprise well-defined, complete bilayers with FC16/βME. The charged component, DOPG, incorporates into the outer monolayer leaflet in the same ratio as provided in the immersion solution but is excluded from the inner leaflet. In all cases that we investigated here, the average area densities of the lipids within the bilayers were close to those in free bilayer membranes. Particularly for charged phospholipids, FC16 provides a distinct advantage over WC14 in the formation of well-defined stBLMs.

Acknowledgment. Support by the National Institute of Standards and Technology (U.S. DOC) in providing the neutron research facilities used in this work is gratefully acknowledged. T.N. was supported by the SURF program funded in part by the NSF (DMR-0454672). This work was further supported by the NSF (CBET-0555201) and the American Health Assistance Foundation (A2008-307). Fruitful discussions with Duncan McGillivray, Gintaras Valincius and support from Paul Kienzle in software implementation are gratefully acknowledged.

LA8033275